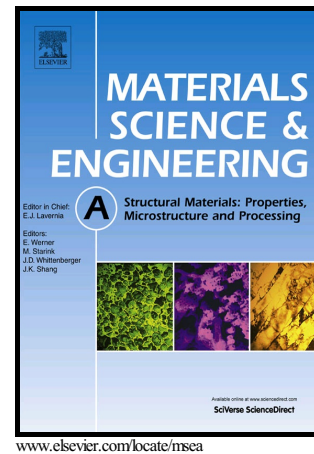


# Author's Accepted Manuscript

On the microstructure and mechanical properties of an Fe-10Ni-7Mn martensitic steel processed by high-pressure torsion

Faezeh Javadzadeh Kalahroudi, Hamidreza Koohdar, Hamidreza Jafarian, Yi Haung, Terence. G. Langdon, Mahmoud Nili-Ahmadabadi



PII: S0921-5093(19)30163-7  
DOI: <https://doi.org/10.1016/j.msea.2019.02.002>  
Reference: MSA37521

To appear in: *Materials Science & Engineering A*

Received date: 14 September 2018  
Revised date: 20 January 2019  
Accepted date: 1 February 2019

Cite this article as: Faezeh Javadzadeh Kalahroudi, Hamidreza Koohdar, Hamidreza Jafarian, Yi Haung, Terence. G. Langdon and Mahmoud Nili-Ahmadabadi, On the microstructure and mechanical properties of an Fe-10Ni-7Mn martensitic steel processed by high-pressure torsion, *Materials Science & Engineering A*, <https://doi.org/10.1016/j.msea.2019.02.002>

This is a PDF file of an unedited manuscript that has been accepted for publication. As a service to our customers we are providing this early version of the manuscript. The manuscript will undergo copyediting, typesetting, and review of the resulting galley proof before it is published in its final citable form. Please note that during the production process errors may be discovered which could affect the content, and all legal disclaimers that apply to the journal pertain.

# On the microstructure and mechanical properties of an Fe-10Ni-7Mn martensitic steel processed by high-pressure torsion

Faezeh Javadzadeh Kalahroudi <sup>a</sup>, Hamidreza Koohdar <sup>a</sup>, Hamidreza Jafarian <sup>b</sup>, Yi Haung <sup>c, d</sup>,  
Terence. G. Langdon <sup>c</sup>, Mahmoud Nili-Ahmadabadi <sup>a, e, \*</sup>

<sup>a</sup> School of Metallurgy and Materials Engineering, University of Tehran, P.O. Box 14395-731, Tehran, Iran

<sup>b</sup> School of Metallurgy and Materials Engineering, Iran University of Science and Technology, Tehran, Iran

<sup>c</sup> Materials Research Group, Department of Mechanical Engineering, University of Southampton, Southampton SO17 1BJ, UK

<sup>d</sup> Department of Design and Engineering, Faculty of Science and Technology, Bournemouth University, Poole, Dorset BH12 5BB, UK

<sup>e</sup> Center of Excellence for High Performance Materials, School of Metallurgy and Materials Engineering, University of Tehran, Tehran, Iran

## Abstract

High-pressure torsion (HPT) processing was applied to an Fe-10Ni-7Mn (wt.%) martensitic steel at room temperature and the grain size was reduced from an initial value of  $\sim 5.5 \mu\text{m}$  to an ultrafine value of  $\sim 185 \text{ nm}$  for the ferritic phase and around  $30 \text{ nm}$  for the austenitic phase after 20 HPT turns. The microstructure and mechanical properties of the as-processed material were evaluated using X-ray diffraction (XRD), electron backscatter diffraction (EBSD), field emission scanning electron microscopy (FESEM), microhardness measurements and tensile testing. In addition, annealing of an as-processed specimen was analyzed by differential scanning calorimetry (DSC). The results show that HPT processing increases the hardness and ultimate tensile strength to  $\sim 690 \text{ Hv}$  and  $\sim 2230 \text{ MPa}$ , respectively, but the ductility is decreased from  $\sim 16.5\%$  initially to  $\sim 6.4\%$  and  $\sim 3.1\%$  after 10 and 20 turns, respectively. The hardness distributions and EBSD images show that a reasonably homogeneous microstructure is formed when applying a sufficient level of pressure and torsional strain. The DSC results demonstrate that processing by HPT reduces the start and finish temperatures of the reverse transformation of martensite to austenite and there is continuous re-crystallization after the recovery process.

**Keywords:** Fe-Ni-Mn martensitic steel; High-pressure torsion; Mechanical properties; Microstructural evolution; Reverse transformation; Severe plastic deformation.

\* Corresponding author

E-mail address: [nili@ut.ac.ir](mailto:nili@ut.ac.ir) (M. Nili-Ahmadabadi)

Tel.: 098-2182084078

## 1. Introduction

The Fe-10Ni-7Mn (wt.%) low carbon martensitic steel is classified as an ultra-high strength steel which exhibits adequate ductility in the solution annealed (SA) condition. However, this excellent age-hardenable steel suffers from post-aging intergranular embrittlement along prior austenite grain boundaries [1, 2]. Recent efforts have focused on the effects of adding alloying elements [3, 4], intercritical annealing [5, 6] and also employing various severe plastic deformation methods to improve the alloy ductility after aging [7, 8].

Severe plastic deformation (SPD) techniques are excellent procedures for fabricating ultrafine-grained (UFG) and/or nano-crystalline (NC) structures by imposing significant magnitudes of plastic strain in various metals and alloys [9, 10]. Numerous specific microstructural features have been extensively reported in SPD-processed materials, including high concentrations of vacancies, exceptional dislocation densities and large fractions of high-angle grain boundaries having non-equilibrium characteristics. Therefore, these materials have the potential for displaying unique properties in strength, ductility and superplasticity compared to their customary coarse-grained counterparts [11].

To date, several SPD processing methods have been applied to Fe-10Ni-7Mn steel such as equal-channel angular pressing (ECAP) [12], severe cold rolling [13, 14] and repetitive corrugation and straightening by rolling (RCSR) [15]. The results reveal that by 85% severe cold rolling the ultimate tensile strength increases to ~950 MPa but the elongation to failure decreases to ~14% [12]. In addition, a 29% increase in the ultimate tensile strength and a reduction in ductility to ~12% appears in this steel after ECAP processing [12]. The same trend was observed also after RCSR processing with an improvement in strength up to ~908 MPa together with a reduction in elongation to failure of ~8.6% [15].

According to these earlier studies, grain refinement by SPD methods in Fe-10Ni-7Mn martensitic steel is frequently accompanied by a phase transformation of martensite to austenite due to a deformation-induced reverse transformation [8]. It was demonstrated by X-ray diffraction (XRD) and differential scanning calorimetry (DSC) that 60% of cold rolling supplied the driving force required for the reverse transformation of martensite to austenite [13]. It is noteworthy to mention that austenite stability at room temperature is also related to the grain size after SPD processing which may hinder the austenite to martensite transformation. An induced austenite transformation after 60% and more of cold rolling enhances the mechanical properties of aged Fe-Ni-Mn and prevents intergranular embrittlement.

In recent decades, several investigations have examined the effect of processing by high-pressure torsion (HPT) on the microstructure and mechanical properties of different iron-based alloys. Thus, it was demonstrated that the microstructure and hardness become uniform after several turns and also there is a hardness saturation at the periphery of the sample disks which is attributed to the high dislocation density and small grain size [16, 17]. The occurrence of phase transformations and epsilon martensite formation after HPT straining in iron-based alloys was discussed in several reports [18-20] wherein the HPT-induced phase changes from  $\gamma$ -austenite into  $\epsilon$ - and  $\alpha'$ -martensites with a  $\gamma \rightarrow \epsilon \rightarrow \alpha'$  sequence. Furthermore, the thermal stability and stored energy in severely deformed 316L stainless steel after HPT processing was studied recently and it was shown that the nano-crystalline specimens exhibit very good thermal stability such that, even after heat treatments executed up to 1000 K, the samples have high dislocation densities and ultrafine grains of less than 200 nm [21, 22].

Although there are several studies related to SPD methods for the Fe-10Ni-7Mn (wt.%) martensitic steel, it appears that there are no reports of the HPT processing of this alloy.

Accordingly, HPT processing was applied on this martensitic steel to achieve a smaller grain size, to inspect any phase transformation and consequently to improve the mechanical properties by a straining in torsion. Since the deformation mode and the amount of strain imposed by HPT are different from other SPD processes, it is reasonable to anticipate that there will be different microstructures and mechanical properties. The present research was therefore initiated with the objective of clarifying the microstructural evolution, mechanical properties and thermal stability of the Fe-10Ni-7Mn (wt.%) martensitic steel when processed by HPT at room temperature.

## 2. Material and experimental methods

An Fe-10Ni-7Mn (wt.%) steel, with a chemical composition as listed in Table 1, was prepared by melting in a vacuum induction melting (VIM) furnace and then remelting in a vacuum arc remelting (VAR) furnace. Afterwards, hot forging was performed on the re-melted ingot at 1423 K and then the ingot was homogenized in a vacuum furnace at 1473 K for 24 h, solution annealed at 1423 K for 1 h and finally quenched in cold water to obtain a fully martensitic microstructure. Samples were cut in the shape of small disks with dimensions of 10 mm diameter and 0.8 mm thickness for use in HPT processing. The processing was conducted at room temperature under an applied pressure of 6.0 GPa with a rotation rate of 1 rpm for totals,  $N$ , of 1, 3, 6, 10 and 20 turns using a facility operating under quasi-constrained conditions [23]. Phase analyses were performed by X-ray diffraction using Cu-K $\alpha$  radiation within angular ranges of 40-100°  $2\theta$  and the microstructure was characterized by field emission scanning electron microscopy (FESEM) using an electron backscatter diffraction (EBSD) detector (the observation position is indicated in Fig. 1).

Vickers microhardness measurements were carried out across the diameters of each disk with distances of 1 mm between each indentation (as marked in Fig. 1) using loads of 100 gf and

dwel times of 10 s. For tensile testing, as shown in Fig. 1, small specimens were cut from the HPT disks at off-center positions with gauge lengths of 1.8 mm, widths of 0.8 mm and thicknesses of 0.5 mm. This method follows the conventional procedure of measuring the tensile properties of the HPT-processed samples by using specimens cut specifically to avoid the region of zero strain at the center of each disk. The tensile experiments were carried out at room temperature with initial strain rates of  $5 \times 10^{-4} \text{ s}^{-1}$  using a SANTAM tensile testing machine. The fracture surfaces of the broken tensile specimens were examined by FESEM. In order to evaluate the thermal stability and phase transformation temperatures of the HPT-processed specimens, calorimetric analyses were performed using a differential scanning calorimetry with a heating rate of  $300 \text{ }^\circ\text{C}/\text{min}$  up to  $600^\circ\text{C}$  in an argon gas environment. To study the change of the stored energy, the heat absorbed or released during the DSC analysis was calculated by integrating the area under each peak.

### 3. Experimental results

#### 3.1. Microstructure and phase evolution after HPT processing

The X-ray diffraction patterns of the specimens in the solution annealed condition and after 1, 3 and 20 turns of HPT processing are shown in Fig. 2(a). The results demonstrate that the microstructure in the SA condition includes only the martensite phase. According to Fig. 2(a), no reversed austenite peak is detected in the HPT-processed specimens and, even with increasing numbers of turns up to  $N = 10$ , it is clear that no phase transformation is induced by HPT processing from martensite ( $\alpha'$ ) to austenite ( $\gamma$ ). The (110) XRD peaks for the SA sample and the HPT-processed specimen after 20 turns are overlapped and magnified in Fig. 2(b) and it is readily apparent that the first martensite peak becomes broadened after the HPT processing.

Grain boundary maps superimposed on phase maps are displayed in Fig. 3 for (a) the SA and (b-d) the HPT-processed specimens, where the martensite and austenite phases are depicted in pink and green colors and the black and red lines correspond to high-angle grain boundaries (HAGBs) and low-angle grain boundaries (LAGBs), respectively. The average grain sizes and the volume fractions of the phases obtained from the EBSD results in the SA and HPT-processed specimens are shown in Table 2 with the grain sizes estimated using the linear intercept method. As anticipated, the HPT processing significantly decreases the grain size in the materials from 5.5  $\mu\text{m}$  in the SA sample to  $\sim 185$  nm for ferrite and about 30 nm for austenite after 20 turns. Finer martensitic grains during HPT are rather problematic by comparison with austenitic since martensite is associated with a high dislocation density that makes it difficult to identify dislocation generation as the main source of grain fragmentation. In contrast to the XRD results in Fig. 2(a), the EBSD data reveal a very small fraction of austenitic phase after HPT processing with the volume fraction tending to increase with increasing numbers of turns.

### *3.2. Mechanical properties after HPT processing*

The evaluation of Vickers microhardness,  $H_v$ , across the specimens' diameters is shown in Fig. 4 for different numbers of HPT turns, where each experimental point corresponds to the mean of five separate measurements. It is readily apparent that there is a significant increase in the hardness values with increasing numbers of turns and in the initial stages of straining the hardness is inhomogeneous throughout the diameters of the disks with higher hardness values recorded near the peripheries. At the maximum straining after 20 turns, the degree of inhomogeneity is reduced. For all straining conditions the measured hardness near the edge of each disk is close to  $\sim 690$   $H_v$ .

The engineering stress-strain curves of the SA and the HPT-processed specimens at room temperature are plotted in Fig. 5 and the values of the ultimate tensile strength (UTS), yield strength (YS) and fracture strain for the different testing conditions are summarized in Table 3. For the SA sample, the UTS and fracture strain were recorded as ~815 MPa and ~16.5%, respectively, whereas after 3 turns the UTS and YS increased to ~1840 and ~1800 MPa, respectively, with a corresponding reduction in the fracture strain to ~10.2%. With increasing numbers of HPT turns, the strength was marginally increased but the elongation was even further reduced to only ~3.1% after 20 turns.

The fracture surfaces of the SA and HPT-processed samples after tensile testing are shown in Fig. 6 where the SA sample in Figs 7(a-b) shows ductile fracture due to the dimple morphology in which the dimples exhibit different sizes and depths. The fracture behavior transforms from ductile to a combination of brittle and ductile after HPT processing as shown in Figs 6(c-j) and after 20 turns several shear bands and cracks are visible in the fracture surface as shown in Fig. 6(g-j).

### *3.3. Thermal stability and phase transformation temperatures after HPT processing*

Figure 7 displays the DSC curves of the SA sample and the HPT-processed specimen after 20 turns during continuous heating up to 600 °C using a heating rate of 300°C/min. Several phase transformations occur during this heating and these transformations are denoted by numbers in the plot. In the SA condition an endothermic peak and three exothermic peaks are present whereas in the HPT-processed sample there are four exothermic and two endothermic peaks. These DSC curves demonstrate that most of the peaks in the SA condition are smaller with less stored energy than in the HPT-processed sample.

## 4. Discussion

### 4.1. Importance of the reverse martensite to austenite transformation

The EBSD images reveal that in the SA condition the sample microstructure contains a lath martensitic phase with a large fraction of LAGBs due to the initial high concentration of dislocations (Fig. 3(a)). The HPT processing transforms a significant fraction of the LAGBs to HAGBs [24] and produces elongated martensitic grains oriented along the shear direction of the HPT straining (Figs 3(b,c)). This is consistent with the general trends associated with microstructural evolution in metals subjected to SPD processing [25]. Finally, after 20 turns the microstructure is composed of a mixture of equiaxed and elongated martensitic grains (Fig. 3(d)).

Based on the EBSD phase maps it is apparent that the HPT processing induces a small fraction of austenite phase in the initial martensitic microstructure. Earlier reports demonstrated the possibility of a reverse transformation of martensite to austenite in SPD processing [8, 13, 26] where the reverse transformation occurs if the applied stress on the material supplies sufficient driving force in terms of chemical and non-chemical elements. The chemical driving force originates from the difference in the Gibbs free energies in the original and the new phases while the non-chemical driving force corresponds to the energy required for nucleation and growth of the new phase [8]. During HPT processing, a part of the mechanical work transforms to heat so that the specimen temperature increases [27]. Furthermore, the anvil pressure produces a significant reduction in the equilibrium phase transformation temperature according to the Clausius-Clapeyron equation [28]. On the other hand, the lath martensite contains a high dislocation density and during the reverse transformation the dislocation energies are released to

some extent as a result of the austenite formation. In practice, it is established that these various factors reduce the required driving force and promote the reverse transformation [8].

The low stacking fault energy (SFE) of the steel may promote an hcp-martensite formation before the reverse austenite transformation [26]. It is reported that in this martensitic steel the transformation of bcc-martensite to hcp-martensite can be achieved at a pressure of 4.3 GPa at room temperature. In addition, earlier investigations show that the hcp-martensite is metastable and could transform to austenite by applying further straining [26]. Therefore, as there is no evidence for hcp-martensite in the XRD analysis and EBSD results even after the first turn of HPT processing, it is concluded that the required pressure for the hcp-martensite to austenite transformation may be supplied by applying severe torsional straining. This behavior is in agreement with another report [18] in which the  $\epsilon$  phase acts as an intermediate phase in the  $\alpha' \rightarrow \gamma$  transformation.

It is reasonable to assume that, by applying additional HPT turns, the stored deformation energy will increase so that larger fractions of austenite may be formed. As shown in Table 2, after 20 turns the austenite content was measured as about 6% and in practice it is difficult to detect this constituent by XRD at levels about 5%. Accordingly, the ultrafine size of the austenite reduces the chance of detection by XRD as shown in Fig. 2(a). On the other hand, as it can be seen in Table 2, that the volume fraction of austenite is a little higher in the 10-turn HPT-processed sample than after 20 turns. This phenomenon was also observed in another report [29] in which reverse and direct martensitic transformations occurred consecutively. It was suggested that the local increase in temperature and high hydrostatic pressure assisted in advancing the reverse transformation during the deformation process, and by further straining during HPT the reversed austenite was able to again transform to martensite [30]. Moreover, multiple  $\gamma \rightarrow \alpha' \rightarrow \gamma$

→  $\alpha'$  phase transformations were achieved in a SUS 304 stainless steel by applying HPT processing with alternate low and high rotation rates at room temperature [18]. Therefore, a minor  $\gamma \rightarrow \alpha'$  transformation may occur in the 20-turn HPT-processed sample.

The observed peak broadening in the XRD pattern of the sample after 20 turns, as shown in Fig. 2(b), is related to the high imposed shear strain and the increase in dislocation density. It is reasonable to assume that the ultrafine grains of the reversed austenite in the HPT-processed specimen may lead to improved mechanical properties.

#### *4.2. Significance of the mechanical properties after HPT processing*

Based on the microhardness measurements in Fig. 4, and noting also the EBSD images in Fig. 3, it appears that the application of HPT is effective in achieving an almost homogenous microstructure provided the applied pressure and the torsional strain are sufficiently high. Similar conclusions were reached in the processing of pure Fe by HPT after 5 turns [31], 316L austenitic stainless steel after 20 turns [17] and SUS316LN steel after 5 turns [32]. Initially, the hardness improves at the disk periphery due to the very high concentration of dislocations and the associated grain refinement caused by the higher imposed strain in this region. Thereafter, the region of higher hardness gradually expands towards the central part of the sample. The hardness saturates when there is essentially a balance between the increase in hardness due to dislocation accumulation and the reduction in hardness due to recovery [32]. Furthermore, as depicted in Fig. 4, the hardness values in the core regions after higher HPT turns are equivalent to the measured values for the regions near the periphery in the samples with fewer HPT turns. Thus, these regions have similar microstructural properties as well. For example, the measured hardness in the center of the 20-turns HPT-processed sample is similar to the periphery of the 3-

turns sample. As a result, the microstructure investigation of the latter sample also reveals information on the properties of the former sample.

It is important to note that processing of the present alloy by other SPD procedures gave lower ultimate tensile strength but higher ductility by comparison with the use of HPT processing [12, 15]. The strength enhancement after HPT processing is attributed to the high density of dislocations, the high density of shear bands and the ultrafine grains that are introduced in the material. Thus, grain refinement and the reverse transformation during HPT yields exceptional tensile strength with a reasonable level of ductility.

In this research the SA specimen shows values for the YS and UTS which are very close, as shown in Fig. 5, with only minor strain hardening due to the high dislocation density of martensite, while the alloy displays about 15% non-uniform deformation because of the ductile nature of the matrix. However, after 3 HPT turns the YS and UTS increase and even further deformation to 10 turns gives higher strength and a higher strain hardening rate in addition to a more uniform plastic deformation but with a reduction in the total elongation. The increase in the strain rate hardening and the uniform plastic deformation is attributed to the reverse austenite transformation and grain refinement.

During the HPT process, accumulation of deformation-induced vacancies produces small vacancy agglomerations. These agglomerates enlarge with increasing strain. During the tensile testing, shear bands form and generate progressively and the formation and propagation of these bands are revealed by the FESEM images from the fracture surfaces of specimens after HPT processing as shown in Fig. 6(i, j). As the shear bands have higher strains compared to the bulk material, more defects and correspondingly higher free energies are created in these regions [33]. This excess free energy supplies the required driving force for void formation during the shear

deformation. As the shear deformation develops, if the local maximum shear stress exceeds the shear yield stress then the voids gradually transform to submicrometer or even micro-cracks [15] and these defects may reduce the overall ductility and affect the fracture behavior during tensile deformation.

#### *4.3. An examination of the fracture behavior after tensile testing*

As is apparent from Fig. 6(a-j), there is a transition in the fracture mode from necking to shearing when the sample is subjected to higher numbers of HPT turns [33]. The fracture structures after HPT processing consist of fragments which are both parts of the martensitic laths and shear bands which appear as a result of deformation accompanied by extremely fine dimples that are direct evidence for ductile fracture [34]. During the HPT process, small cave-like shear bands are produced [35] which are displayed in greater detail in Fig. 6(j). Additionally, the dimples are of the scale of the grain size. The excessive reduction in the dimple size in the HPT-processed sample by comparison with the SA sample appears to be a consequence of the very high energetic and distorted microstructure in the samples after HPT processing [15]. This duplex behavior was reported also in a medium-carbon steel after applying 5 HPT turns where there was non-uniform deformation with a fracture surface having separate fragments of  $\sim 2\text{-}5\ \mu\text{m}$  width with dimples developed within them [34]. It was concluded from these earlier experiments that the tensile strain accumulated on the laths of the martensite plates split the material along the grain boundaries and produced deep pits on the fracture surface [34].

#### *4.4. Significance of the DSC curves*

Based on the DSC curves in Fig. 7, the phase transformations and their start and finish temperatures may be obtained during continuous heating of the specimen. In the initial condition,

the exothermic processes at 231-27 °C, 369-402°C and 402-435°C are respectively corresponded to recovery through the annihilation of dislocations and vacancies and to the multi-stage formation of precipitates [5]. The endothermic process, which is related to the austenite formation, starts at 545°C and is not complete even at the end of heating. By contrast, after HPT processing the temperature ranges for the exothermic processes change to 231-285°C, 357-401°C and 401-416°C, respectively, and a single re-crystallization peak appears at 285-357°C. In SPD materials, the stored energy is usually sufficiently high to provide recovery followed by continuous re-crystallization [36]. Moreover, HPT processing may produce ultra-fine grains with boundaries having high angles of misorientation and with high densities of crystalline defects which act as re-crystallization nuclei [37, 38]. Two endothermic peaks are also visible which are related to the reversion of precipitates to austenite by a diffusional mechanism and the reverse transformation of the martensitic matrix to austenite by a diffusionless shear mechanism at 510-535°C and 535-580°C, respectively [5, 6]. It can be observed that the start temperature of austenite formation is decreased about 35°C after the HPT processing (Fig. 7). Large fractions of crystalline defects may also promote the reverse transformation of martensite to austenite by acting as nucleation sites [39].

The enthalpy calculation of the DSC peaks reveals that the released heat during the recovery process is increased to about 4 times after the HPT processing. In the SA sample, the sum of the released heat related to the exothermic peaks is calculated at about 0.85 J/g. This value increases to about 3.85 J/g after 20 turns of HPT processing. Another report shows that for a 316L austenitic stainless steel the released heat from the exothermic peak increases from 1.4 J/g to 4.9 J/g after applying 10 turns of HPT [21]. These changes imply the effect of the severe deformation on enhancing the released energy. For the endothermic peak in the SA sample, it

was not possible to calculate the area under the peak due to the limitation in the annealing temperature range. After 20 turns of HPT processing it should be noted that, although the peaks of the austenite formation appear in this range but with different mechanisms of formation due to diffusional and diffusionless shear mechanisms, the overall calculation of the phase transformation enthalpy is not very accurate.

## 5. Summary and conclusions

1. An Fe-10Ni-7Mn (wt.%) martensitic steel was processed by HPT at room temperature. This processing reduced the grain size from an initial value of  $\sim 5.5 \mu\text{m}$  in the solution annealed sample to  $\sim 210$  and  $\sim 185$  nm for ferrite and about 30 nm for austenite after 6 and 20 HPT turns, respectively.

2. The results show that the reverse transformation of martensite to austenite occurs even after one HPT turn. By further straining, the volume fraction of the reversed austenite increases and finally reaches  $\sim 6\%$  after 20 turns. This grain refinement and reverse transformation leads to higher tensile strength with a reasonable ductility. A homogenous ultrafine-grained structure with a saturation hardness of  $\sim 690$  Hv was achieved after processing through 20 turns of HPT.

3. In tensile testing, the fracture behavior changes from fully ductile in the initial solution annealed condition to a mixture of brittle and ductile after HPT processing. HPT processing followed by annealing causes a continuous re-crystallization after recovery and a reduction in the start and finish temperatures of the reverse martensitic transformation due to the large numbers of defects produced during the deformation process which act as nucleation sites.

## Acknowledgment

One of the authors (H. Koohdar) express his thanks to Iran National Science Foundation (INSF) for partial financial support of this research.

## References

- [1].S.H. Nedjad, M.N. Ahmadabadi, T. Furuvara, Correlation between the intergranular brittleness and precipitation reactions during isothermal aging of an Fe–Ni–Mn maraging steel, *Materials Science and Engineering: A* 490(1-2) (2008) 105-112. <https://doi.org/10.1016/j.msea.2008.01.070>.
- [2].S.H. Nedjad, M.N. Ahmadabadi, T. Furuvara, Transmission electron microscopy study on the grain boundary precipitation of an Fe-Ni-Mn maraging steel, *Metallurgical and Materials Transactions A* 39(1) (2008) 19-27. <https://doi.org/10.1007/s11661-007-9407-z>.
- [3].S. Hosseinnedjad, J. Teimouri, A. Tahmasebifar, H. Shirazi, M. Niliahadabadi, A new concept in further alloying of Fe–Ni–Mn maraging steels, *Scripta Materialia* 60(7) (2009) 528-531. <https://doi.org/10.1016/j.scriptamat.2008.11.046>.
- [4].F. Forghani, M. Nili-Ahmadabadi, Microstructural characteristics and second-phase particles in yttrium-bearing Fe-10Ni-7Mn martensitic steels, *Journal of Rare Earths* 32(4) (2014) 326-333. [https://doi.org/10.1016/s1002-0721\(14\)60075-2](https://doi.org/10.1016/s1002-0721(14)60075-2).
- [5].H. Shirazi, G. Miyamoto, S. Hossein Nedjad, H. Ghasemi-Nanesa, M. Nili Ahmadabadi, T. Furuvara, Microstructural evaluation of austenite reversion during intercritical annealing of Fe–Ni–Mn martensitic steel, *Journal of Alloys and Compounds* 577 (2013) S572-S577. <https://doi.org/10.1016/j.jallcom.2012.02.015>.
- [6].H. Koohdar, M. Nili-Ahmadabadi, M. Habibi-Parsa, H.R. Jafarian, T. Bhattacharjee, N. Tsuji, On the Stability of Reversely Formed Austenite and Related Mechanism of Transformation in an Fe-Ni-Mn Martensitic Steel Aided by Electron Backscattering Diffraction and Atom Probe Tomography, *Metallurgical and Materials Transactions A* 48(11) (2017) 5244-5257. <https://doi.org/10.1007/s11661-017-4288-2>.

- [7]. M. Nili Ahmadabadi, H. Shirazi, H. Ghasemi-Nanesa, S. Hossein Nedjad, B. Poorganji, T. Furuwara, Role of severe plastic deformation on the formation of nanograins and nano-sized precipitates in Fe–Ni–Mn steel, *Materials & Design* 32(6) (2011) 3526-3531. <https://doi.org/10.1016/j.matdes.2011.02.018>.
- [8]. H. Ghasemi-Nanesa, M. Nili-Ahmadabadi, H.R. Koohdar, M. Habibi-Parsa, S. Hossein Nedjad, S.A. Alidokht, T.G. Langdon, Strain-induced martensite to austenite reverse transformation in an ultrafine-grained Fe–Ni–Mn martensitic steel, *Philosophical Magazine* 94(13) (2014) 1493-1507. <https://doi.org/10.1080/14786435.2014.886785>.
- [9]. R.Z. Valiev, R.K. Islamgaliev, I.V. Alexandrov, Bulk nanostructured materials from severe plastic deformation, *Progress in materials science* 45(2) (2000) 103-189. [https://doi.org/10.1016/S0079-6425\(99\)00007-9](https://doi.org/10.1016/S0079-6425(99)00007-9).
- [10]. A. Azushima, R. Kopp, A. Korhonen, D.Y. Yang, F. Micari, G.D. Lahoti, P. Groche, J. Yanagimoto, N. Tsuji, A. Rosochowski, A. Yanagida, Severe plastic deformation (SPD) processes for metals, *CIRP Annals* 57(2) (2008) 716-735. <https://doi.org/10.1016/j.cirp.2008.09.005>.
- [11]. R.Z. Valiev, Y. Estrin, Z. Horita, T.G. Langdon, M.J. Zehetbauer, Y. Zhu, Producing Bulk Ultrafine-Grained Materials by Severe Plastic Deformation: Ten Years Later, *Jom* 68(4) (2016) 1216-1226. <https://doi.org/10.1007/s11837-016-1820-6>.
- [12]. H. Shirazi, M. Nili-Ahmadabadi, A. Fatehi, S. Hossein Nedjad, Effect of Severe Plastic Deformation on Mechanical Properties of Fe-Ni-Mn High Strength Steel, *Advanced Materials Research* 83-86 (2009) 16-23. <https://doi.org/10.4028/www.scientific.net/AMR.83-86.16>.
- [13]. H. Koohdar, M. Nili-Ahmadabadi, M. Habibi-Parsa, H. Ghasemi-Nanesa, Investigating on the Reverse Transformation of Martensite to Austenite and Pseudoelastic Behavior in Ultrafine-Grained Fe-10Ni-7Mn (wt %) Steel Processed by Heavy Cold Rolling, *Advanced Materials Research* 829 (2013) 25-29. <https://doi.org/10.4028/www.scientific.net/AMR.829.25>.
- [14]. H.R. Koohdar, M. Nili-Ahmadabadi, M. Habibi-Parsa, H.R. Jafarian, H. Ghasemi-Nanesa, H. Shirazi, Observation of pseudoelasticity in a cold rolled Fe–Ni–Mn martensitic steel, *Materials Science and Engineering: A* 658 (2016) 86-90. <https://doi.org/10.1016/j.msea.2016.01.113>.

- [15]. A. Mirsepasi, M. Nili-Ahmadabadi, M. Habibi-Parsa, H. Ghasemi-Nanesa, A.F. Dizaji, Microstructure and mechanical behavior of martensitic steel severely deformed by the novel technique of repetitive corrugation and straightening by rolling, *Materials Science and Engineering: A* 551 (2012) 32-39. <https://doi.org/10.1016/j.msea.2012.04.073>.
- [16]. A. Vorhauer, R. Pippan, On the homogeneity of deformation by high pressure torsion, *Scripta Materialia* 51(9) (2004) 921-925. <https://doi.org/10.1016/j.scriptamat.2004.04.025>.
- [17]. M. El-Tahawy, J. Gubicza, Y. Huang, H.L. Choi, H.M. Choe, J.L. Lábár, T.G. Langdon, Evolution of Microstructure, Phase Composition and Hardness in 316L Stainless Steel Processed by High-Pressure Torsion, *Materials Science Forum* 879 (2016) 502-507. <https://doi.org/10.4028/www.scientific.net/MSF.879.502>.
- [18]. J.G. Li, M. Umemoto, Y. Todaka, K. Tsuchiya, Formation of Ultrafine Grained Structure in SUS 304 Stainless Steel Produced by High Pressure Torsion (HPT), *Materials Science Forum* 561-565 (2007) 847-852. <https://doi.org/10.4028/www.scientific.net/MSF.561-565.847>.
- [19]. R.B. Figueiredo, F.L. Sicupira, L.R.C. Malheiros, M. Kawasaki, D.B. Santos, T.G. Langdon, Formation of epsilon martensite by high-pressure torsion in a TRIP steel, *Materials Science and Engineering: A* 625 (2015) 114-118. <https://doi.org/10.1016/j.msea.2014.11.091>.
- [20]. J. Gubicza, M. El-Tahawy, Y. Huang, H. Choi, H. Choe, J.L. Lábár, T.G. Langdon, Microstructure, phase composition and hardness evolution in 316L stainless steel processed by high-pressure torsion, *Materials Science and Engineering: A* 657 (2016) 215-223. <https://doi.org/10.1016/j.msea.2016.01.057>.
- [21]. M. El-Tahawy, Y. Huang, T. Um, H. Choe, J.L. Lábár, T.G. Langdon, J. Gubicza, Stored energy in ultrafine-grained 316L stainless steel processed by high-pressure torsion, *Journal of Materials Research and Technology* 6(4) (2017) 339-347. <https://doi.org/10.1016/j.jmrt.2017.05.001>.
- [22]. M. El-Tahawy, Y. Huang, H. Choi, H. Choe, J.L. Lábár, T.G. Langdon, J. Gubicza, High temperature thermal stability of nanocrystalline 316L stainless steel

- processed by high-pressure torsion, *Materials Science and Engineering: A* 682 (2017) 323-331. <https://doi.org/10.1016/j.msea.2016.11.066>.
- [23]. R.B. Figueiredo, P.R. Cetlin, T.G. Langdon, Using finite element modeling to examine the flow processes in quasi-constrained high-pressure torsion, *Materials Science and Engineering: A* 528(28) (2011) 8198-8204. <https://doi.org/10.1016/j.msea.2011.07.040>.
- [24]. Y. Huang, M. Lemang, N.X. Zhang, P.H.R. Pereira, T.G. Langdon, Achieving superior grain refinement and mechanical properties in vanadium through high-pressure torsion and subsequent short-term annealing, *Materials Science and Engineering: A* 655 (2016) 60-69. <https://doi.org/10.1016/j.msea.2015.12.086>.
- [25]. Y. Cao, S. Ni, X. Liao, M. Song, Y. Zhu, Structural evolutions of metallic materials processed by severe plastic deformation, *Materials Science and Engineering: R: Reports* 133 (2018) 1-59. <https://doi.org/10.1016/j.mser.2018.06.001>.
- [26]. H. Ghasemi-Nanesa, M. Nili Ahmadabadi, H. Shirazi, S. Hossein Nedjad, Observation of Reverse Transformation of  $\alpha$ - $\epsilon$ - $\gamma$  in ultrafine - grained Fe-Ni-Mn Age Hardenable Martensitic Steel, *International Journal of Modern Physics: Conference Series* 05 (2012) 9-17. <https://doi.org/10.1142/s201019451200178x>.
- [27]. K. Edalati, Y. Hashiguchi, P.H.R. Pereira, Z. Horita, T.G. Langdon, Effect of temperature rise on microstructural evolution during high-pressure torsion, *Materials Science and Engineering: A* 714 (2018) 167-171. <https://doi.org/10.1016/j.msea.2017.12.095>.
- [28]. Y. Ivanisenko, I. Maclaren, X. Sauvage, R. Valiev, H. Fecht, Shear-induced  $\alpha \rightarrow \gamma$  transformation in nanoscale Fe-C composite, *Acta Materialia* 54(6) (2006) 1659-1669. <https://doi.org/10.1016/j.actamat.2005.11.034>.
- [29]. I. Kabanova, V. Sagaradze, Statistical analysis of mutual misorientations of austenite (martensite) crystals after  $\gamma \rightarrow \alpha \rightarrow \gamma$  ( $\alpha \rightarrow \gamma \rightarrow \alpha$ ) martensitic transformations, *The Physics of Metals and Metallography* 88(2) (1999) 143-151.
- [30]. I.Y. Litovchenko, A. Tyumentsev, M. Zahozheva, A. Korznikov, Direct and reverse martensitic transformation and formation of nanostructured states during severe plastic deformation of metastable austenitic stainless steel, *Rev. Adv. Mater. Sci* 31 (2012) 47-53.

- [31]. Y. Todaka, Y. Miki, M. Umemoto, C.H. Wang, K. Tsuchiya, Tensile Property of Submicrocrystalline Pure Fe Produced by HPT-Straining, *Materials Science Forum* 584-586 (2008) 597-602. <https://doi.org/10.4028/www.scientific.net/MSF.584-586.597>.
- [32]. S. Shi, Z. Zhang, X. Wang, G. Zhou, G. Xie, D. Wang, X. Chen, K. Ameyama, Microstructure evolution and enhanced mechanical properties in SUS316LN steel processed by high pressure torsion at room temperature, *Materials Science and Engineering: A* 711 (2018) 476-483. <https://doi.org/10.1016/j.msea.2017.11.064>.
- [33]. Y.Z. Tian, J.J. Li, P. Zhang, S.D. Wu, Z.F. Zhang, M. Kawasaki, T.G. Langdon, Microstructures, strengthening mechanisms and fracture behavior of Cu–Ag alloys processed by high-pressure torsion, *Acta Materialia* 60(1) (2012) 269-281. <https://doi.org/10.1016/j.actamat.2011.09.058>.
- [34]. M.V. Karavaeva, S.K. Kiseleva, M.M. Abramova, A.V. Ganeev, R.Z. Valiev, Microstructure, properties, and failure characteristics of medium-carbon steel subjected to severe plastic deformation, *IOP Conference Series: Materials Science and Engineering* 63 (2014) 012056. <https://doi.org/10.1088/1757-899x/63/1/012056>.
- [35]. C. Ruffing, A. Kobler, E. Courtois-Manara, R. Prang, C. Kübel, Y. Ivanisenko, E. Kerscher, Fatigue Behavior of Ultrafine-Grained Medium Carbon Steel with Different Carbide Morphologies Processed by High Pressure Torsion, *Metals* 5(2) (2015) 891-909. <https://doi.org/10.3390/met5020891>.
- [36]. A. Belyakov, K. Tsuzaki, Y. Kimura, Y. Mishima, Annealing behavior of a ferritic stainless steel subjected to large-strain cold working, *Journal of Materials Research* 22(11) (2011) 3042-3051. <https://doi.org/10.1557/jmr.2007.0398>.
- [37]. Y. Ivanisenko, R.K. Wunderlich, R.Z. Valiev, H.J. Fecht, Annealing behaviour of nanostructured carbon steel produced by severe plastic deformation, *Scripta Materialia* 49 (2003) 947-952. [https://doi.org/10.1016/s1359-6462\(03\)00478-0](https://doi.org/10.1016/s1359-6462(03)00478-0).
- [38]. A. Belyakov, T. Sakai, H. Miura, R. Kaibyshev, K. Tsuzaki, Continuous recrystallization in austenitic stainless steel after large strain deformation, *Acta Materialia* 50 (2002) 1547-1557. [https://doi.org/10.1016/S1359-6454\(02\)00013-7](https://doi.org/10.1016/S1359-6454(02)00013-7).
- [39]. S. Chen, A. Shibata, L.J. Zhao, S. Gao, Y.Z. Tian, N. Tsuji, Microstructural evolution of metastable austenitic steel during high-pressure torsion and subsequent heat

treatment, IOP Conference Series: Materials Science and Engineering 63 (2014) 012053.  
<https://doi.org/10.1088/1757-899x/63/1/012053>.

### Figure Captions

Fig. 1. Schematic of the HPT sample, dimensions and positions of the tensile specimen, hardness measurements and microstructure observation

Fig. 2. (a) X-ray diffraction patterns of the solution annealed and HPT-processed specimens, (b) magnified (110) XRD peaks for solution annealed sample and HPT-processed specimen after 20 turns.

Fig. 3. EBSD phase maps for samples (a) solution annealed and HPT-processed for (b) 1, (c) 6, (d) 20 turns.

Fig. 4. Microhardness distributions recorded across the diameters of the solution annealed and HPT-processed samples.

Fig. 5. Engineering stress-strain curves of solution annealed and HPT-processed samples.

Fig. 6. FESEM images of fracture surfaces in the solution annealed sample (a, b), HPT-processed specimens after 3 turns (c, d), 10 turns (e, f), 20 turns (g- j).

Fig. 7. DSC curves of the solution annealed sample and HPT-processed specimen after 20 turns at a heating rate of  $300\text{ }^{\circ}\text{C min}^{-1}$ .

**Table captions**

Table. 1. Chemical composition of the steel.

Table. 2. Average grain size and volume fraction of the phases obtained from EBSD results.

Table. 3. Values of ultimate tensile strength, yield strength and fracture strain for the solution annealed and HPT-processed samples.

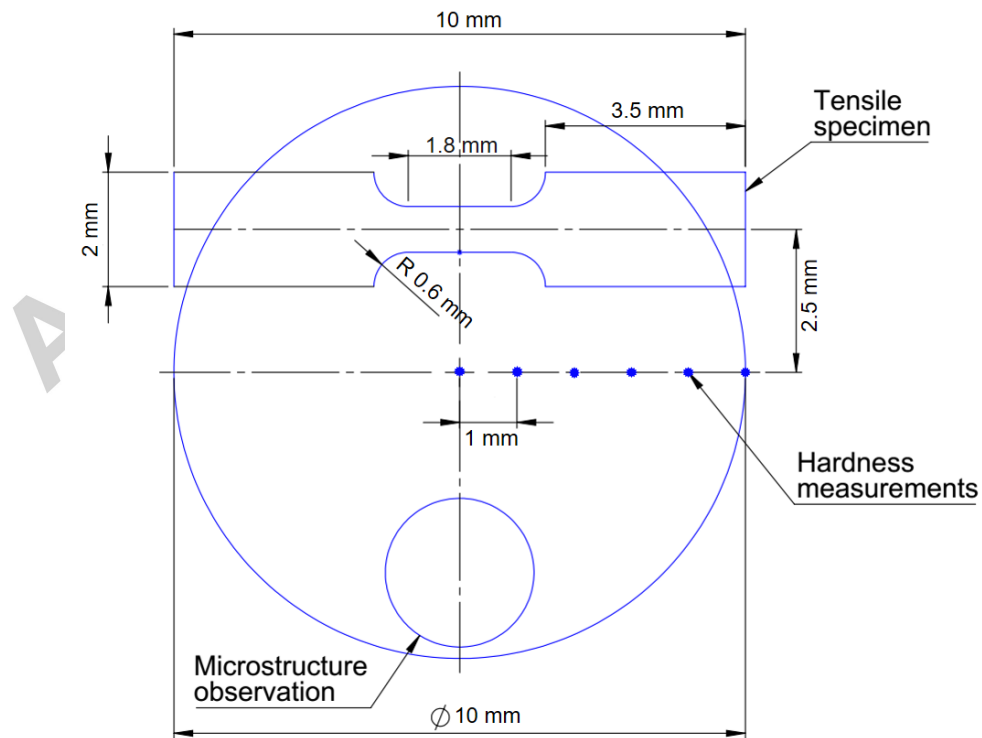


Fig. 1. Schematic of the HPT sample, dimensions and positions of the tensile specimen, hardness measurements and microstructure observation

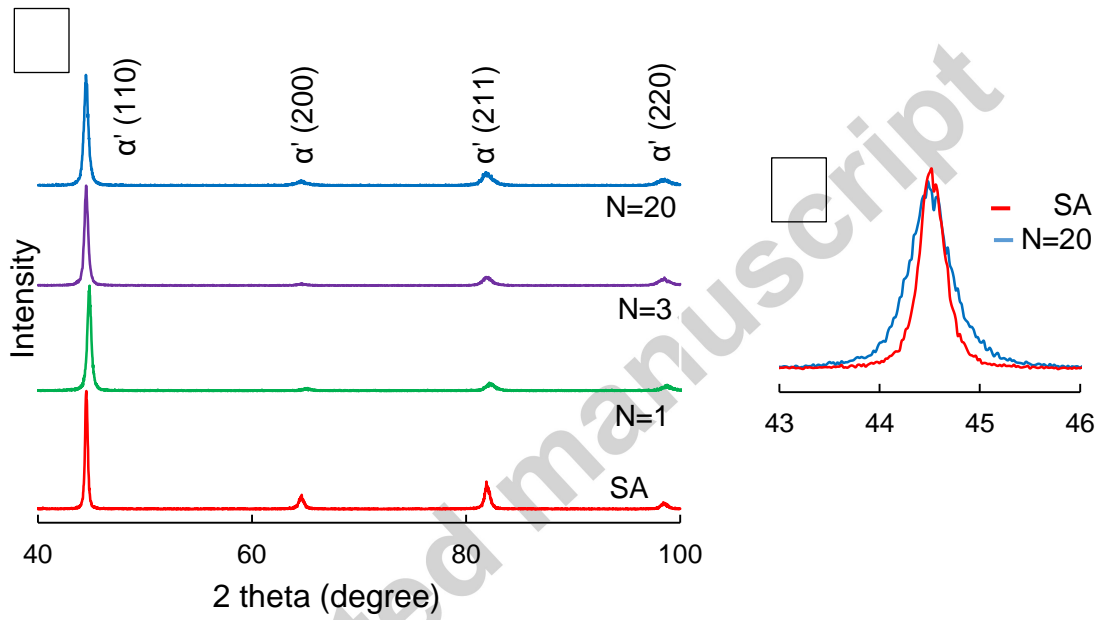
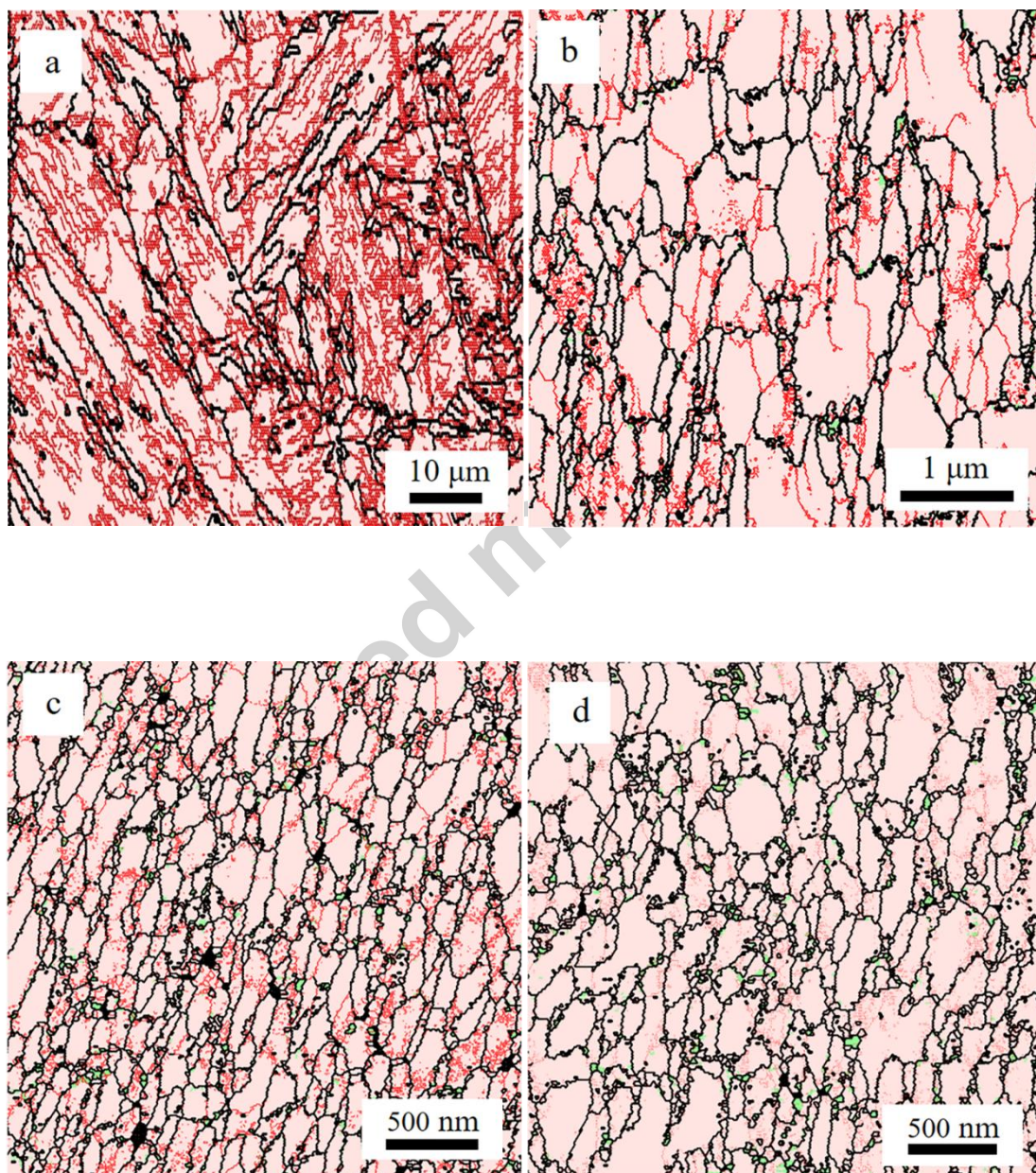


Fig. 2. (a) X-ray diffraction patterns of the solution annealed and HPT-processed specimens, (b) magnified (110) XRD peaks for solution annealed sample and HPT-processed specimen after 20 turns.



—  $\theta \geq 15^\circ$   
—  $2^\circ \leq \theta < 15^\circ$

□  $\alpha'$ -martensite  
□ austenite

Fig. 3. EBSD phase maps for samples (a) solution annealed and HPT-processed for (b) 1, (c) 6,  
(d) 20 turns.

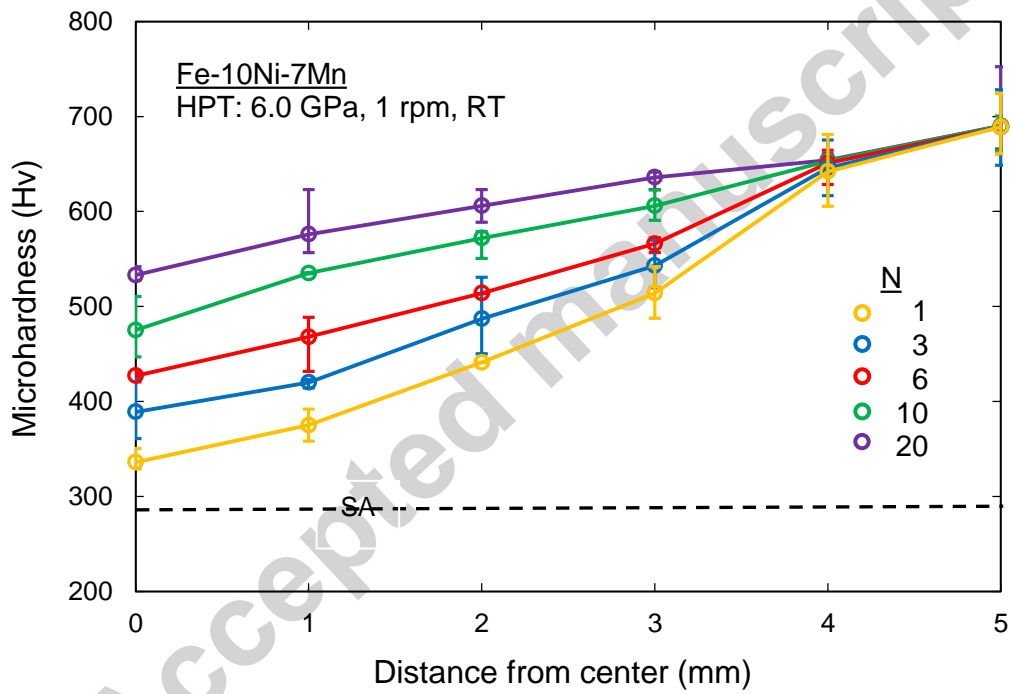


Fig. 4. Micro-hardness distribution recorded across the diameter of the solution annealed and  
HPT-processed samples.

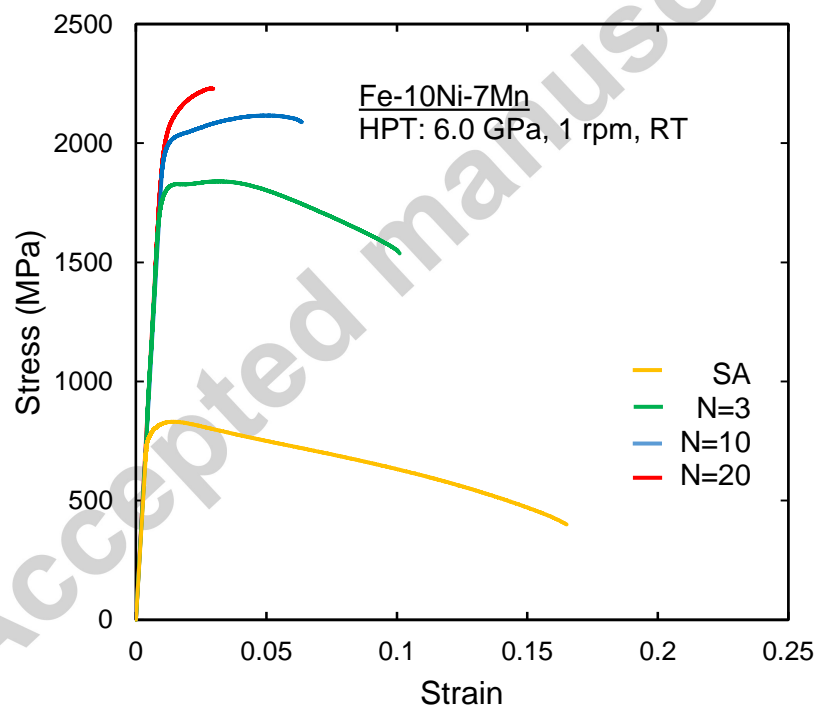
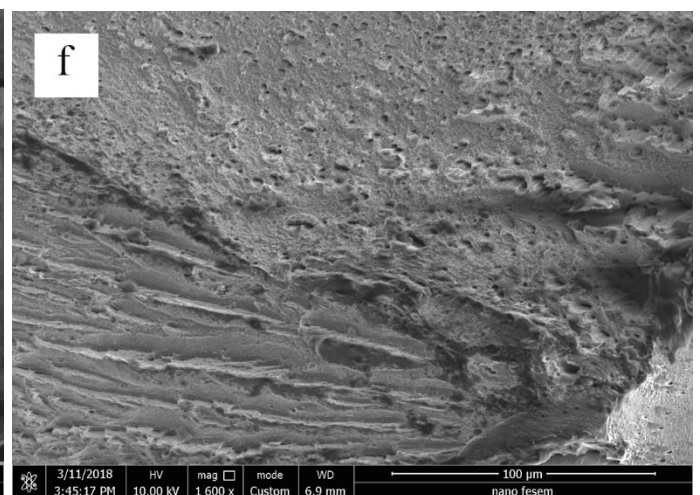
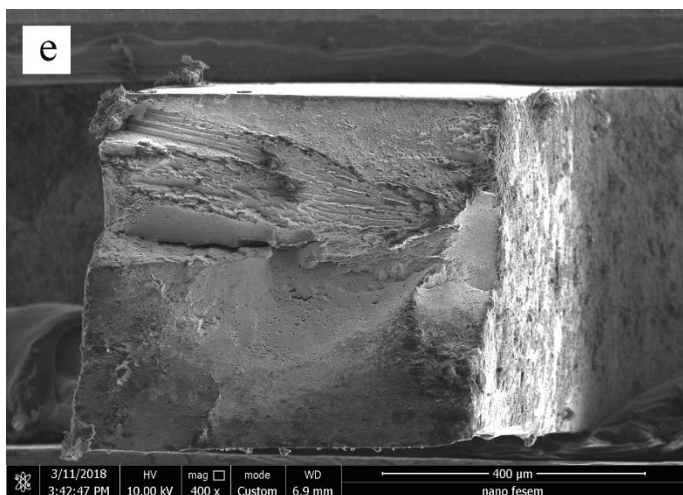
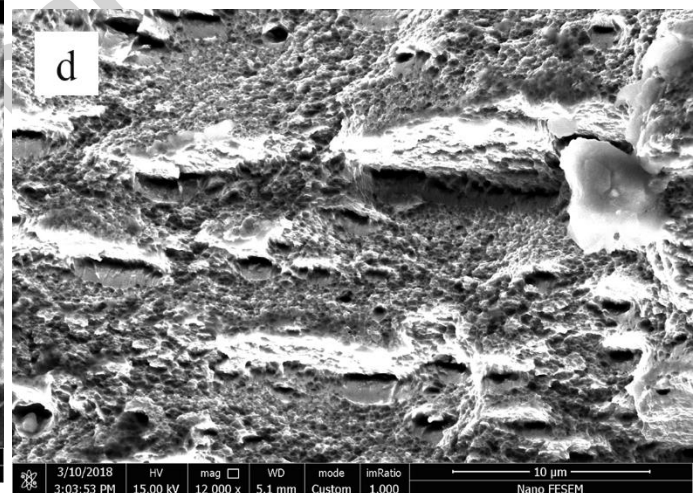
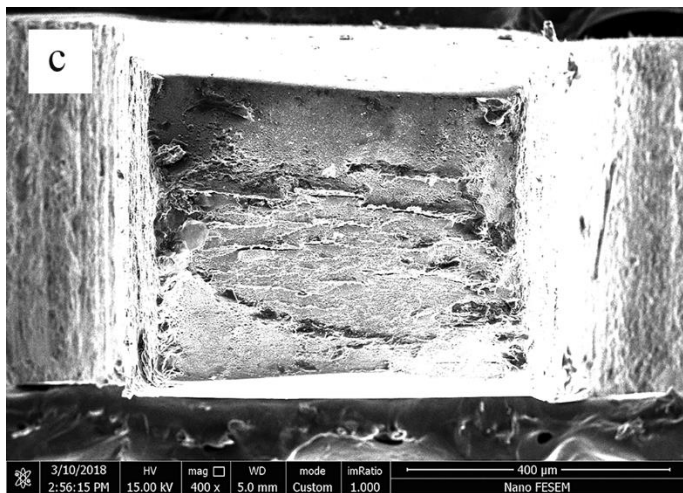
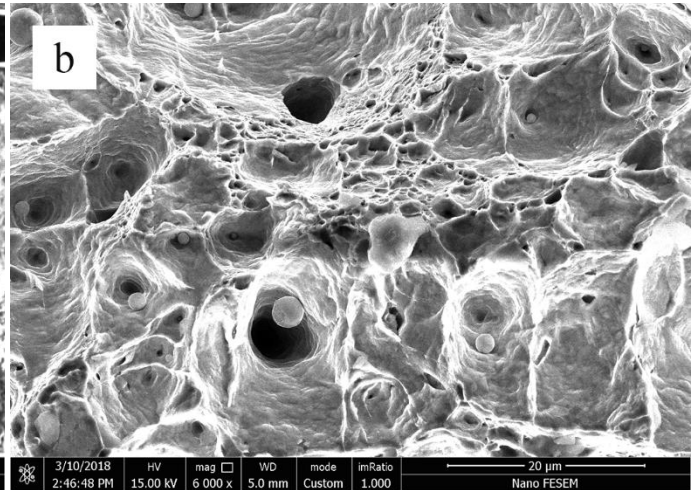
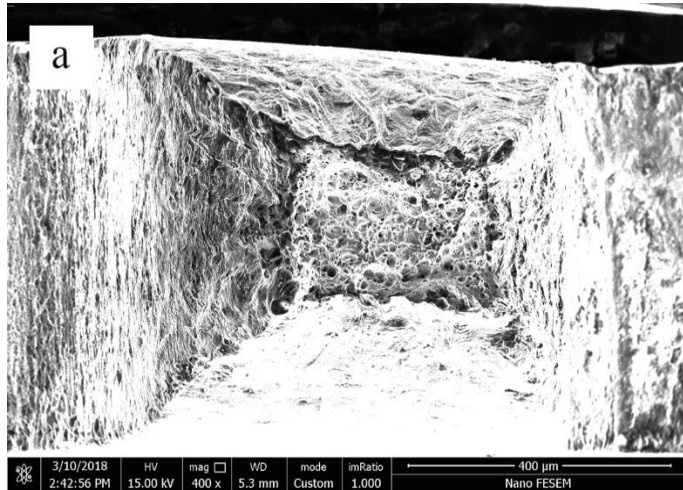


Fig. 5. Engineering stress-strain curves of solution annealed and HPT-processed samples.



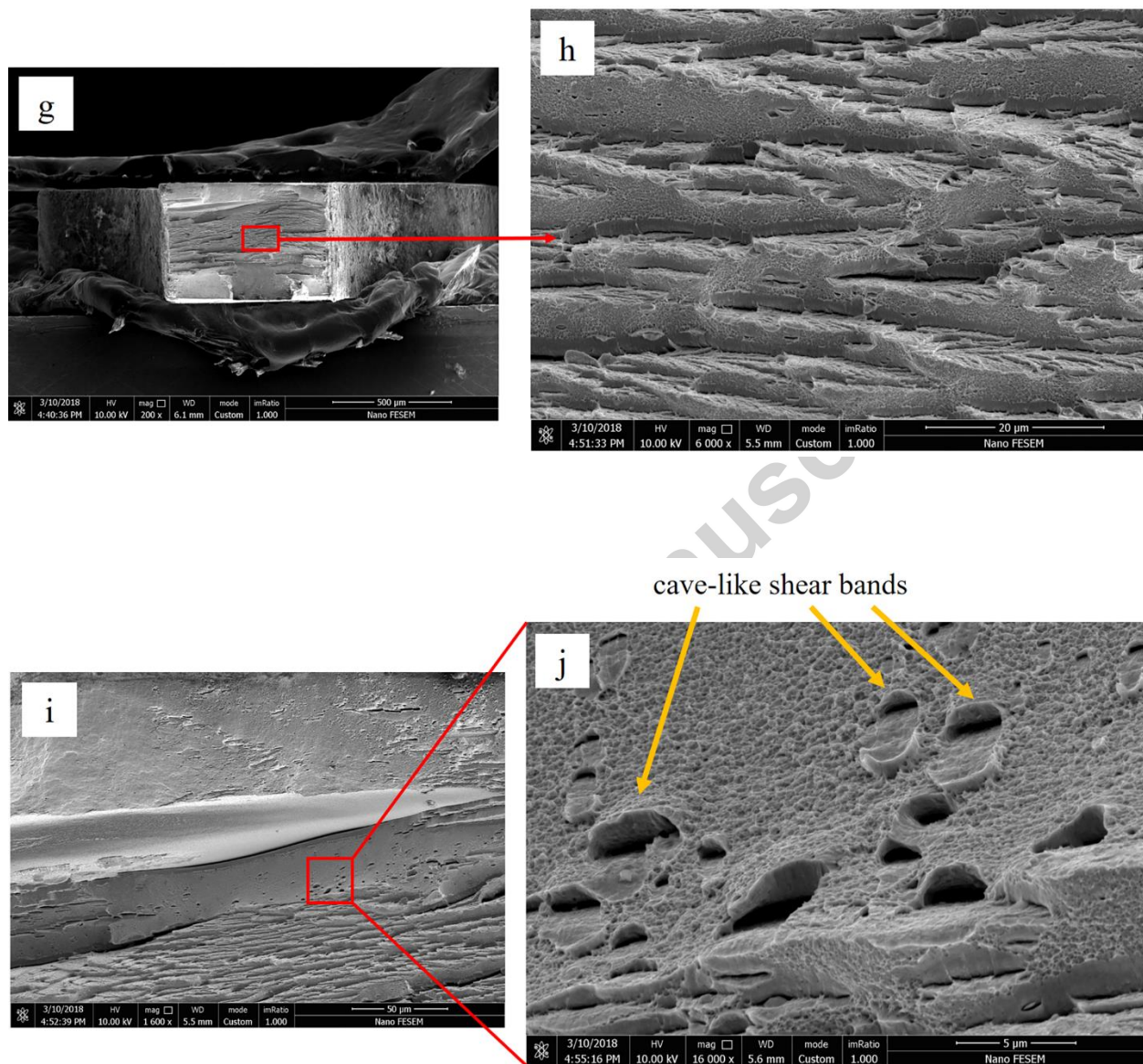


Fig. 6. FESEM images of fracture surfaces in the solution annealed sample (a, b), HPT-processed specimens after 3 turns (c, d), 10 turns (e, f), 20 turns (g- j).

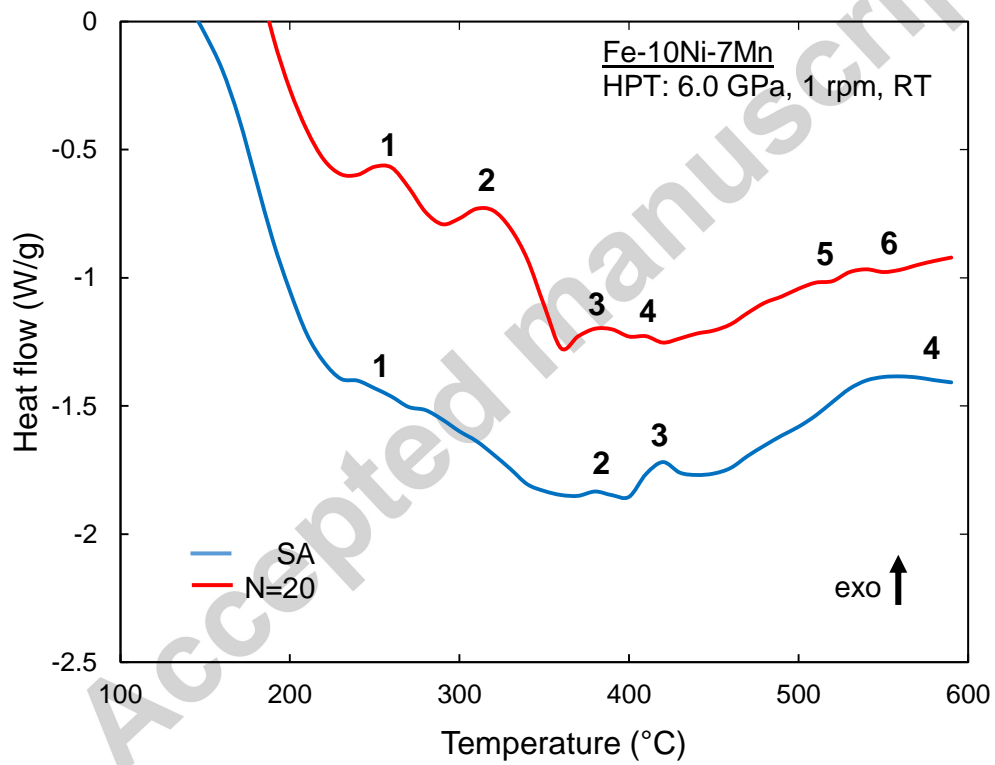


Fig. 7. DSC curves of the solution annealed sample and HPT-processed specimen after 20 turns at a heating rate of  $300\text{ }^{\circ}\text{C min}^{-1}$ .

Table. 1. Chemical composition of the studied steel.

Element	Fe	Ni	Mn	C	S	P	N	Al
wt%	Bal.	10.05	6.97	0.005	0.006	0.005	0.005	0.003

Table. 2. Average grain size and volume fraction of the phases obtained from EBSD results.

	Martensite- $\alpha'$ (vol. %)	Austenite- $\gamma$ (vol. %)	Martensite- $\alpha'$ Grain size (nm)	Austenite- $\gamma$ Grain size (nm)
SA	100	0	□ 5500	-
N=1	98±0.5	2±0.5	□ 630	□ 70
N=6	95±1	5±1	□ 210	□ 35
N=10	92.5±1	7.5±1	□ 200	□ 30
N=20	94±1	6±1	□ 185	□ 28

Table. 3. Values of ultimate tensile strength, yield strength and fracture strain for the solution annealed and HPT-processed samples.

	UTS (MPa)	YS (MPa)	Fracture strain (%)
SA	815	790	16.5
N=3	1840	1800	10.2
N=10	2115	1995	6.4
N=20	2230	2040	3.1

Accepted manuscript